Spatial distribution of dopants and oxygen-related defects in antimony-doped Czochralski silicon

Sébastien Dubois, Wei Han, Nicolas Enjalbert, Adrien Danel, Yichun Wang

Spatial distribution of dopants and oxygen-related defects in antimony-doped Czochralski silicon

Sébastien Dubois[1], Wei Han[2], Nicolas Enjalbert[1], Adrien Danel[1], Yichun Wang[2]

[1]Univ. Grenoble Alpes, CEA, Liten, Campus INES, 73375 Le Bourget du Lac, France

[2]LONGi Green Energy Technology Co., Ltd., Xi'an 710000, Shaanxi, China

Abstract

Antimony (Sb)-doped Czochralski (Cz)-grown silicon (Si) wafers would feature superior performances in comparison with the conventional phosphorus (P)-doped wafers and start to be deployed into mass production. However, published studies about the properties of Sb-doped wafers for solar cells are rather scarce. This work investigates the spatial (i.e., axial and radial) distributions of Sb, interstitial oxygen (O_i) and oxygen thermal donors (TD), in Sb-doped Cz ingots processed with melt recharging (RCz), focusing on wafers representative of the whole RCz cycle. This study confirmed first the interest in Sb-doping for obtaining Si ingots and wafers with a controlled and narrowed resistivity range. Furthermore, the studied wafers featured low as-grown TD concentrations, low enough not to affect the bulk carrier lifetime (τ_b). Results also showed that Sb-doping does not significantly influence the TD formation kinetics. Last, the studied wafers featured relatively low O_i concentrations ($[O_i]$) below 7×10^{17} cm^{-3} for most samples, with rather flat $[O_i]$ radial profiles. As these Sb-doped samples also presented low Thermal History Index values, they should not be prone to O-related defects-induced τ_b degradations during high temperature steps.

KEYWORDS: silicon, solar cell, ingot, Czochralski, antimony, oxygen, defect

1. INTRODUCTION

With the massive deployment of passivated contacts solar cells into mass production and photovoltaic (PV) conversion efficiency values still improving despite performances now close to the theoretical limit for crystalline silicon (Si) single-junction devices [1], the requirements regarding the electronic properties of n-type Czochralski (Cz) Si are more and more severe. Nowadays, n-type Si wafers are essentially doped with phosphorus (P) atoms. However, antimony (Sb) doping could feature advantages over this conventional P doping. Sb acts as a donor element in crystalline Si. Sb has a relatively low equilibrium segregation coefficient (k_0) between solid and liquid Si, of 0.023 (in comparison P has a k_0 of 0.35) [2]. This low k_0 should induce significant resistivity (ρ) variations along the height of Sb-doped Cz ingots (i.e., ρ divided by 2 between the first solidified fraction and a solidified fraction of 0.75) [2]. Nevertheless, Sb in molten Si is highly volatile. Depending on the ingot pulling conditions (e.g., pressure, gas flow), the Sb evaporation from the free surface of the melt can compensate or over-compensate the solid-liquid segregation effects. This can result in Sb concentration ([Sb]) variations along the height of the ingot that can significantly differ from those expected by considering segregation mechanisms only. For instance, ingots with ρ values increasing from the top (first solidified region) to the bottom parts can be obtained [2]. Recently, LONGi showed that it was possible to control these effects and developed a specific melt Recharging Cz (RCz) process for Sb doping [3]. This industrial process results in n-type wafers for high efficiency solar cells featuring a tight and controlled ρ distribution.

Despite this important advantage (which in particular facilitates process fine-tuning) and the first deployments of Sb-doped wafers into mass production, published studies about the properties of Sb-doped Si wafers for solar cells are rather scarce. This contribution investigates the spatial distribution (i.e., axial along the length of the ingot and radial across the diagonal of a wafer) of Sb, interstitial oxygen (O_i) and oxygen (O)-related thermal donors

(TD), in Sb-doped RCz ingots and wafers. This is particularly important since O-related defects are still among the main recombination centers involved in bulk carrier lifetime (τ_b) limitations in advanced Cz-Si wafers [4].

2. EXPERIMENTAL DETAILS

This study focuses on the first (R1), the fourth (R4) and the last (R7) ingots from an industrial RCz cycle (i.e., 7 ingots pulled from the same silica crucible via melt recharging). As shown in Figure 1, these ingots were then cut in bricks (5 to 6 bricks per ingot, the length of a given ingot being usually over 3 m). For each ingot, at both extremities (i.e., seed and tail sides) 2 mm-thick wafers (i.e., slabs) were prepared for Fourier Transform Infrared Spectroscopy (FTIR) in order to extract the O_i and substitutional carbon (C_s) concentrations ($[O_i]$ and $[C_s]$, respectively). The FTIR analyses were conducted in the center of the slabs. The different bricks were cut in M10 size (i.e., 182×182 mm^2) 150 µm-thick wafers. Then for each ingot, series of consecutive wafers were extracted from the top (T: Brick 1, a-side), middle (M: Brick 3, b-side) and bottom (B: last brick, b-side) bricks (see Figure 1). The labelling of the wafers is explained in Figure 1.

In order to assess the [Sb], $[O_i]$ and [TD] radial distributions, the procedure described in [5-6] (sometimes referred to as OxyMap) was conducted. This procedure is based on ρ measurements along the wafer diagonal before and after the intentional TD formation and annihilation. Notice that the measurement system was only compliant with M2 (156.75×156.75 mm^2) wafers. Thus, the entire M10 diagonal was reconstructed by using 2 M10 adjacent wafers laser-cut in M2 samples, as shown in Figure 1. This explains why some locations along the M10 diagonal feature two different measurement points. It is worth noticing that all the $[O_i]$ values presented within this work (obtained by FTIR or by OxyMap,

the last being a FTIR-calibrated technique) are provided according to the ASTM F1188-93a standard. The presented [O_i] values are therefore 22% higher than those corresponding to the ASTM F121-83 standard, which is the prevailing standard in the PV industry. Furthermore, some wafers were processed in amorphous Si / crystalline Si heterojunction (SHJ) solar cells by using the fabrication process described in [7]. These wafers did not experience any high temperature steps (such as external gettering steps) before the cell processing. Photoluminescence (PL) images were acquired after the metallization steps.

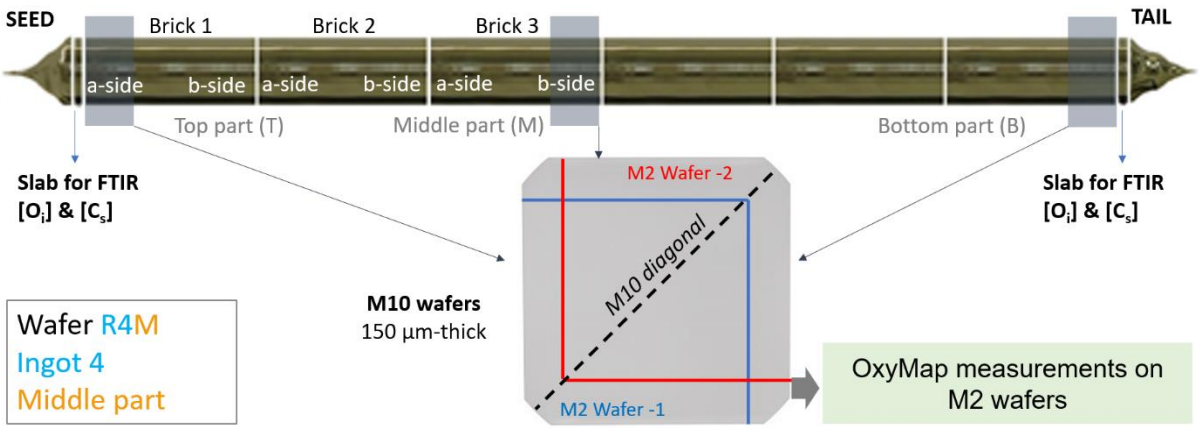

Figure 1. Schematic representation of the procedure used for the preparation and characterization of the samples: ingot cropping (including the preparation of slabs for FTIR analyses), brick sawing and extraction of M10 wafers, laser-cutting of adjacent M10 samples in M2 wafers for OxyMap measurements. The bottom left frame explains the labelling of the samples.

3. RESULTS AND DISCUSSIONS

3.1. Antimony axial and radial distributions

Figure 2 a) presents the radial variations of the ρ after the high temperature step used to annihilate the as-grown TD (i.e., formed during the ingot cooling). Therefore, these ρ

values are directly linked to the [Sb]. First, we can notice that for all wafers, the radial ρ variations feature "V-shape" profiles. Indeed, the solidification usually starts at the edges of a Cz crystal and proceeds towards the center of the crystal, inducing higher dopant concentrations in the center due to segregation effects [2].

It is worth noticing the specific feature of the ρ variation along the height of Sb-doped ingots. Indeed, by focusing on the first ingot (R1), the ρ (center of the wafer) varies from 1.5 Ω.cm (top) to 1.7 Ω.cm (bottom). Thus, the extent of the ρ axial variation is very limited (e.g., in ref. [8] the ρ of a P-doped ingot is divided by 3.6 from the top to the bottom of the ingot). Furthermore, unlike what is observed with P doping, there is a slight increase of ρ from the top to the bottom parts (therefore a [Sb] decrease). Overall, for the whole RCz cycle, the ρ (center of the wafer) features very low variations, in the 1.36 - 2.05 Ω.cm range, confirming the interest of such Sb-doped RCz Si for high efficiency solar cells.

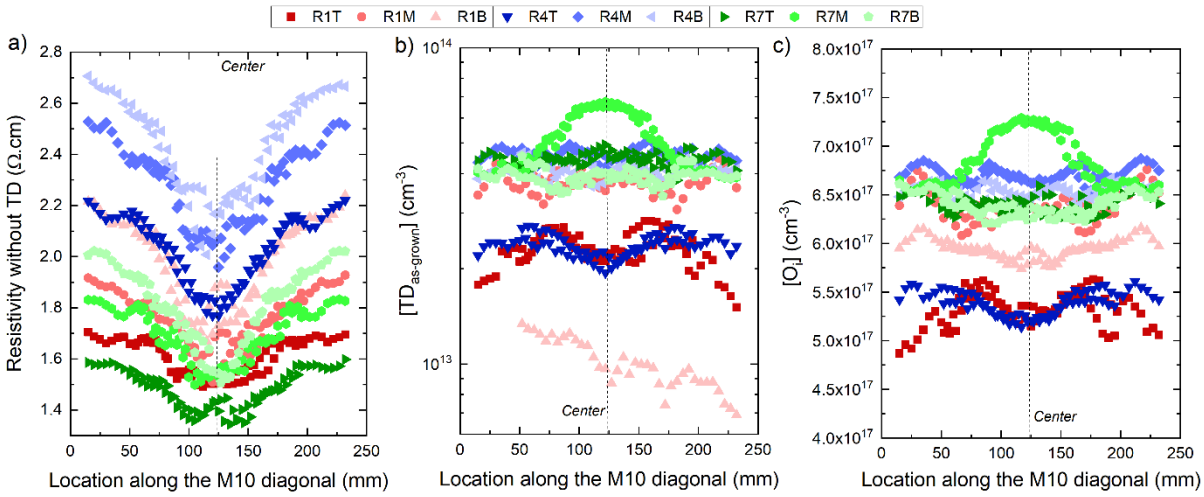

Figure 2. Radial distributions of a) ρ without TD, b) [$TD_{as\text{-}grown}$] and c) [O_i].

3.2. As-grown thermal donors axial and radial distributions

About the radial distribution of the as-grown [TD] ([$TD_{as\text{-}grown}$]) shown in Figure 2 b), it is worth noticing that all the studied samples feature low [$TD_{as\text{-}grown}$], below 7×10^{13} cm^{-3}.

These values are significantly lower than those reported in previous studies [6]. Such low values are probably related to the combination of low [O_i] and the fast cooling of the ingots (as shown later in this contribution). The non-expected [$TD_{as\text{-}grown}$] radial distribution of the R1B sample is likely due to the fact that here the [$TD_{as\text{-}grown}$] are in the vicinity of the detection limit. A particularly fast cooling of the bottom part of the first ingot could be responsible for these low values.

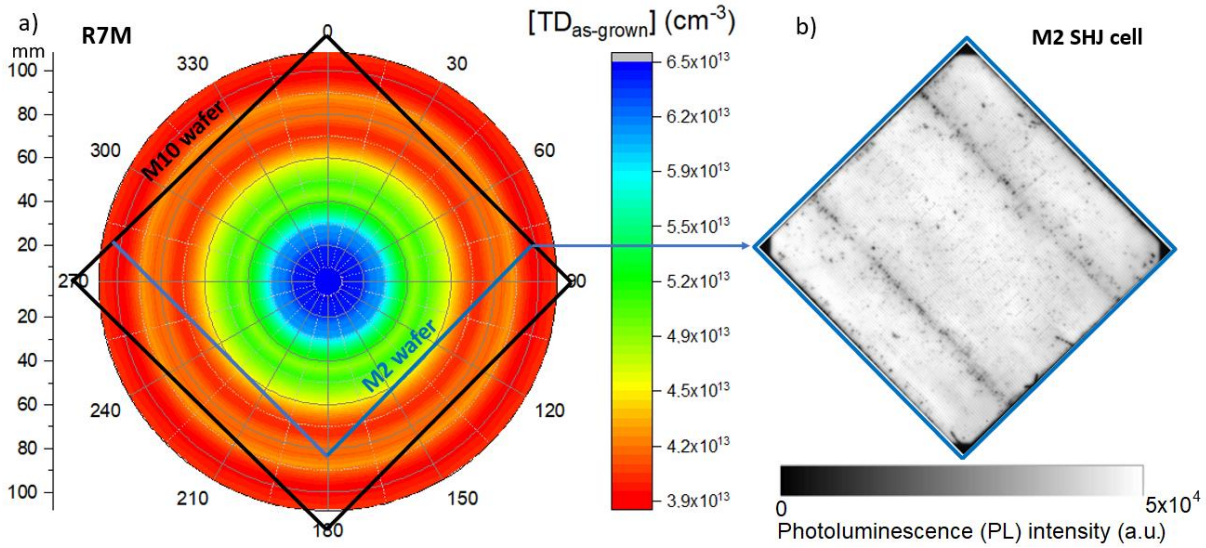

Figure 3. a) 2-D [$TD_{as\text{-}grown}$] mapping of the R7M sample reconstructed from the [$TD_{as\text{-}grown}$] diagonal line scan by assuming a centrosymmetric geometry. The black and blue lines indicate the M10 and M2 wafer dimensions, respectively. b) Photoluminescence image of a M2 SHJ cell processed by using a R7M wafer (without pre-treatment).

In order to assess the impact of the as-grown TD on τ_b, the TD-limited Shockley-Read-Hall (SRH) carrier lifetime (τ_{TD}) for the highest [$TD_{as\text{-}grown}$] found here (sample R7M, center of the wafer) was computed by using the expressions presented in [9] (empirical parametrizations allowing to compute from a given [TD] the input data to be fed into SRH recombination calculations). One of the input parameters for this computation was the equilibrium electron density, which was determined from the ρ (equal to 1.5 Ω.cm) measured

on the sample before the as-grown TD annihilation step. The computed τ_{TD} is equal to 84.7 ms (for an excess carrier density of 10^{15} cm^{-3}). This value is well above the Auger-limited carrier lifetime (equal to 34.9 ms) [10]. Therefore, for all the samples, the τ_b values should not be affected by the as-grown TD. To further assess this hypothesis, a M2 SHJ cell was processed from a R7M wafer (adjacent to the wafers used for the OxyMap measurements). Figure 3 b) presents the PL image of this solar cell. Whereas the 2-dimension (2-D) [$TD_{as-grown}$] mapping shown in Figure 3 a) (reconstructed from the diagonal scan by assuming a centrosymmetric configuration) highlights significant changes in this parameter, the spatial distribution of the PL signal is rather homogenous (except some defectivity due to a non-optimized automation), supporting the fact that the as-grown TD do not impact (at least not significantly) the τ_b values.

3.3. Thermal donor formation kinetics in Sb-doped wafers

The main principle of the OxyMap technique for determining the [O_i] values relies on the strong dependence of the TD formation kinetics on [O_i] [5]. It uses semi-empirical models for the TD formation kinetics established from Boron (B)- and P-doped samples. Therefore, it is necessary to assess the OxyMap compliance with Sb-doped wafers. To that end, the [O_i] extracted from OxyMap were confronted with the values determined from FTIR analyses. As the FTIR analyses were conducted in the center of the slabs, the [O_i] from OxyMap used for this comparison are the values averaged on a length (along the wafer diagonal) of 1 cm in the center of the wafer. Figure 4 presents the [O_i] values obtained by both FTIR and OxyMap. Overall, a good agreement is observed between both values (deviations below 11% for all samples, except the R4T and R7T samples which feature deviations close to 20%). Notice that the presence of carbon, known for slowing-down the TD formation kinetics when [C_s] and [O_i] are in the same order of magnitude [11], cannot be involved for explaining this slight discrepancy. Indeed, for all samples the [C_s] were below the FTIR detection limit (i.e., 5×10^{16}

cm^{-3}). On the one hand, this overall good agreement between both FTIR and OxyMap [O_i] shows that OxyMap can be used with Sb-doped Si wafers. On the other hand, it indirectly demonstrates that the TD formation kinetics are not significantly influenced by Sb doping (at least for the [Sb] studied here). Such a result is first in good agreement with previous studies showing that for non-compensated B- and P-doped Si with dopant concentrations below 10^{16} cm^{-3}, the TD formation kinetics do not depend on the nature and concentration of the doping element, but only on the electron density at the temperature used for TD formation [12-13]. It was even shown that the TD formation kinetics were not influenced by high B and P concentrations (i.e., $>3\times10^{17}$ cm^{-3}) in a p-type B-P compensated material for which the room temperature equilibrium hole concentration was about 10^{16} cm^{-3} [14]. This result is also in good agreement with the fact that neither the O diffusivity [15] nor the low-temperature (i.e., 650°C) Si oxide (SiO_x) precipitation kinetics [16] would be influenced by moderate (i.e., $\leq 4\times10^{16}$ cm^{-3}) [Sb].

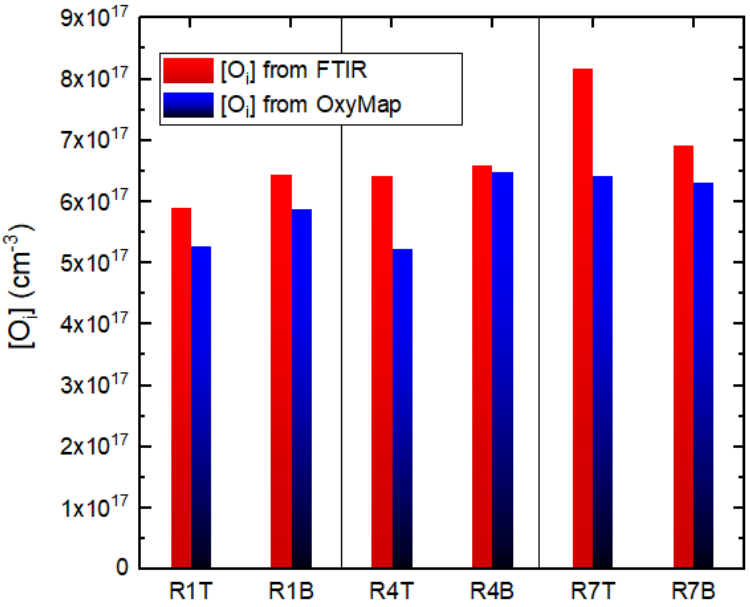

Figure 4. [O_i] extracted from FTIR and OxyMap for the top and bottom parts of the 3 studied Cz ingots.

3.4. Interstitial oxygen axial and radial distributions

Figure 2 c) shows the [O_i] radial variations of the different studied wafers. First, we can notice that most of the samples present low [O_i], below 7×10^{17} cm^{-3}, with even wafers featuring [O_i] below 6×10^{17} cm^{-3}. Overall, the radial [O_i] distributions feature rather "flat" profiles (e.g., for R1B [O_i] varies in the 5.7×10^{17} - 6.2×10^{17} cm^{-3} range). There is a notable exception, which concerns the R7M sample (i.e., last ingot, middle part) with [O_i] values significantly higher in the center of the wafer.

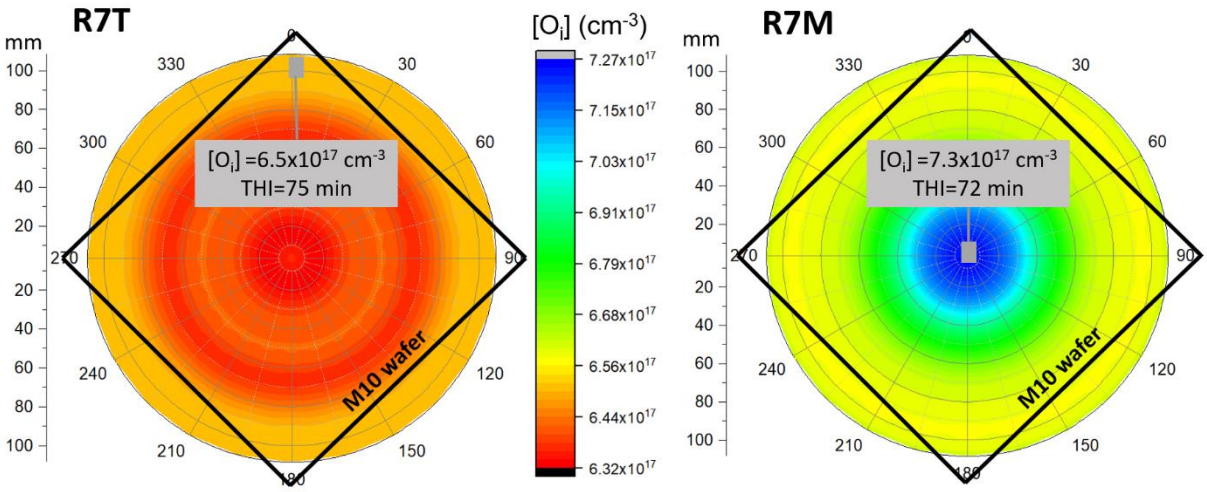

Figure 5. 2-D [O_i] mappings of the R7T (left) and R7M (right) samples reconstructed from the [O_i] diagonal line scans by assuming a centrosymmetric geometry. The black squares indicate the M10 wafer dimensions. The grey frames indicate the [O_i] and THI values extracted at the edge for the R7T sample and in the center for the R7M sample.

It is interesting to assess if the τ_b of the studied Sb-doped wafers could be affected by the formation of recombination active O-related defects (e.g., SiO_x precipates) during the high temperature B-diffusion step used in particular for the processing of TOPCon devices. Such τ_b degradations usually depend on both [O_i] and the Thermal History Index (THI) of the ingot [17]. The later parameter provides a good indicator of the overall thermal history of a given piece of Si and can be computed from the [O_i] and [$TD_{as\text{-}grown}$] values [17]. Figure 5 shows the reconstructed 2-D [O_i] mapping of the R7T and R7M samples. These samples are particularly

interesting for assessing these risks of τ_b degradation. Indeed, the R7T sample corresponds to the top of the ingot and should therefore presents higher THI values. As previously mentioned, the R7M sample features the highest [O_i]. The THI were computed at the periphery of the R7T sample and at the center of the R7M sample (where the [O_i] are the highest, respectively equal to 6.5×10^{17} cm^{-3} and 7.3×10^{17} cm^{-3}). The computed THI values are equal to 75 min (R7T) and 72 min (R7M). According to Veirman et al [17], for a [O_i] value of about 7.5×10^{17} cm^{-3}, if the THI is lower than 200 min, τ_b should not be affected by the formation of recombination active O-related defects. Therefore, the studied samples should not be concerned by such issues. Notice that it will be important to confirm this hypothesis by processing complete TOPCon solar cells, since the thermal budget of the B-diffusion steps currently used for the fabrication of TOPCon devices is different (i.e., higher) than the one used in [16] (boron diffusion step conducted from a BCl_3 precursor, 30 min long drive in at 940°C under N_2, cooling rate of 4.5 °C /min).

4. CONCLUSIONS

This work focused on the spatial (i.e., radial and axial) distribution of dopants and O-related defects in Sb-doped Cz ingots with melt-recharging. This study confirmed first the interest in Sb-doping for obtaining Si ingots and wafers with a controlled and narrowed ρ range. Furthermore, the studied wafers (representative of a whole RCz cycle) featured low [$TD_{as\text{-}grown}$] values, low enough not to affect τ_b. This work also showed that Sb-doping does not significantly influence the TD formation kinetics. Last, the studied wafers featured relatively low [O_i] (below 7×10^{17} cm^{-3} for most samples) with rather flat radial profiles and should not be prone to O-related defects-induced τ_b degradations during high temperature

steps. This last hypothesis should be further assessed by processing complete TOPCon solar cells.

REFERENCES

[1] pv magazine. Longi claims world's highest efficiency for silicon solar cells, 2025. https://www.pv-magazine.com/2025/04/14/longi-claims-worlds-highest-efficiency-for-silicon-solar-cells/

[2] W. Zulenher, Czochralski growth of silicon, J. Cryst. Growth. 65 (1983) 189. DOI: 10.1016/0022-0248(83)90051-9

[3] Y. Wang, A new generation of high-efficiency Si wafers, presented during the: 12th international workshop on Crystalline Silicon for Solar Cells (CSSC), Hangzhou, China, 2024.

[4] G. Li, S. Yuan, S. Zhou, Y. Wu, H. Chen, H. Zhang, C. Wang, L. Wang, X. Yu, D. Yang, Separated striations in n-type Czochralski silicon solar cells, Appl. Phys. Lett. 124 (2024) 252103. DOI: 10.1063/5.0204270

[5] J. Veirman, S. Dubois, N. Enjalbert, M. Lemiti, A fast and easily implemented method for interstitial oxygen concentration mapping through the activation of thermal donors in silicon, Energy Procedia. 8 (2012) 41. DOI: 10.1016/j.egypro.2011.06.099

[6] B. Martel, J. Veirman, M. Cascant, N. Enjalbert, M. Tomassini, R. Peyronnet, J. Stadler, E. Fayard, S. Dubois, G. Raymond, X. Brun, P. Bonnard, Spatial characterization of interstitial oxygen and its related defects in Czochralski silicon wafers and ingots: A way to improve the material and device quality, in: Proceedings of the 42nd IEEE Photovoltaic Specialist Conference (PVSC), New Orleans, LA, USA, 2015, pp. 1-3. DOI: 10.1109/PVSC.2015.7355686

[7] A. Danel, N. Chaugier, J. Veirman, R. Varache, M. Albaric, E. Pihan, Closing the gap between n- and p-type silicon heterojunction solar cells: 24.47% efficiency on lightly doped Ga wafers, Prog. Photovolt. Res. Appl. 31 (2023) 1235. DOI: 10.1002/pip.3635

[8] T. Le, Y. Cai, Z. Yang, R. Chen, D. Macdonald, A. Liu, Industrial Czochralski n-type Silicon Wafers: Gettering Effectiveness and Possible Bulk Limiting Defects, Sol. RRL. 8 (2024) 2300928. DOI: 10.1002/solr.202300928

[9] M. Tomassini, J. Veirman, R. Varache, E. Letty, S. Dubois, Y. Hu, Ø. Nielsen, Recombination activity associated with thermal donor generation in monocrystalline silicon and effect on the conversion efficiency of heterojunction solar cells, J. Appl. Phys. 119 (2016) 084508. DOI: 10.1063/1.4942212

[10] T. Niewelt, B. Steinhauser, A. Richter, B. Veith-Wolf, A. Fell, B. Hammann, N. E. Grant, L. Black, J. Tan, A. Youssef, J. D. Murphy, J. Schmidt, M. C. Schubert, S. W. Glunz, Reassessment of the intrinsic bulk recombination in crystalline silicon, Solar Energy Materials and Solar Cells. 235 (2022) 111467. DOI: 10.1016/j.solmat.2021.111467

[11] Y. M. Babitskii, N. I. Gorbacheva, P. M. Grinshtein, M. A. Ilin, V. P. Kuznetsov, M. G. Milvidskii, B. M. Turovskii, Kinetics of generation of low-temperature oxygen donors in silicon containing isovalent impurities, Soviet Phys. Semicond. 22 (1988) 187.

[12] W. Wijaranakula, Formation kinetics of oxygen thermal donors in silicon, Appl. Phys. Lett. 59 (1991) 1608. DOI: 10.1063/1.106245

[13] K. Wada, Unified model for formation kinetics of oxygen thermal donors in silicon, Phys. Rev. B. 30 (1984) 5884. DOI: 10.1103/PhysRevB.30.5884

[14] F. Tanay, S. Dubois, J. Veirman, N. Enjalbert, J. Stendera, I. Périchaud, Oxygen-related thermal donor formation in dopant-rich compensated Czochralski silicon, IEEE Transactions on Electron Devices. 61 (2014) 1241. DOI: 10.1109/TED.2014.2311832

[15] W. Wijaranakula, J. H. Matlock, H. Mollenkopf, Oxygen diffusion in antimony-doped silicon, Appl. Phys. Lett. 53 (1988) 1068. DOI: 10.1063/1.100068

[16] F. Secco d'Aragona, P. L. Fejes, Oxygen precipitation in antimony-doped silicon wafers, Appl. Phys. Lett. 48 (1986) 665. DOI: 10.1063/1.96737

[17] J. Veirman, B. Martel, E. Letty, R. Peyronnet, G. Raymond, M. Cascant, N. Enjalbert, A. Danel, T. Desrues, S. Dubois, C. Picoulet, X. Brun, P. Bonnard, Thermal history index as a bulk quality indicator for Czochralski solar wafers, Solar Energy Materials and Solar Cells. 158 (2016) 55. DOI: 10.1016/j.solmat.2016.05.051

Figure captions

Figure 1. Schematic representation of the procedure used for the preparation and characterization of the samples: ingot cropping (including the preparation of slabs for FTIR analyses), brick sawing and extraction of M10 wafers, laser-cutting of adjacent M10 samples in M2 wafers for OxyMap measurements. The bottom left frame explains the samples' notation.

Figure 2. Radial distributions of a) ρ without TD, b) [$TD_{as\text{-}grown}$] and c) [O_i].

Figure 3. a) 2-D [$TD_{as\text{-}grown}$] mapping of the R7M sample reconstructed from the [$TD_{as\text{-}grown}$] diagonal line scan by assuming a centrosymmetric geometry. The black and blue lines indicate the M10 and M2 wafer dimensions, respectively. b) Photoluminescence image of a M2 SHJ cell processed by using a R7M wafer (without pre-treatment).

Figure 4. [O_i] extracted from FTIR and OxyMap for the top and bottom parts of the 3 studied Cz ingots.

Figure 5. 2-D [O_i] mappings of the R7T (left) and R7M (right) samples reconstructed from the [O_i] diagonal line scans by assuming a centrosymmetric geometry. The black squares indicate the M10 wafer dimensions. The grey frames indicate the [O_i] and THI values extracted at the edge for the R7T sample and in the center for the R7M sample.